THREE DIMENSIONAL DYNAMIC RESPONSE AND EARTHQUAKE RESISTANT DESIGN OF ROCK FILL DAM AGAINST INPUT EARTHQUAKE IN DIRECTION OF DAM AXIS

by

Masao HAYASHI*, Hiroya KOMADA* and Yoshikazu FUJIWARA*

SYNOPSIS

Past damages of fill type dams have often occured at the abutment during earthquake. The earthquake resistant design in contact zone with side spillway or rock abutment is interested in three dimensional response analysis. Dynamic Young's modulus and coefficient of viscosity of granular rock material are determined by tri-axial dynamic test in laboratory. According to some results in numerical response analysis, destructive tensile stress is apt to occure at slope near the crest and in contact zone with the rock abutment. It is desired that such the stress should be resisted by well compacted soil core or cohesively improved rock fill material.

INTRODUCTION

The behavier of rock fill dam in earthquake may be two dimensional as usual analysis but is more or less three dimensional. For example, the abutments of some dams were damaged in past Tokachi-oki earthquake (1968). Shear stress and normal stress at the abutment of dam have not been by conventional response analysis. Accordingly the earthquake resistant design of the abutment has not been established. Then this paper describes the problems.

1. Characteristics of rock fill material under dynamic repeated deformation

Dynamic tri-axial test was carried out for large specimen of granular material which contains 100mm maximum grain. Distribution of the grain size was similar as actual rock fill dam. The specimen has 50cm in diameter and 50cm in height. Level of static axial stress was chosen less than 10 kg/cm^2. Amplitude of axial dynamic stress was applied to ± 0.5 kg/cm^2 and its frequencies was 0.01 to 6 hz. Lateral pressure was keeped static. Dynamic elasticity Ed (fig. 1) and dynamic viscosity η (fig. 3) during assumed heavy earthquake were obtained from dynamic hysterisis loop (fig. 2). Static Young's modulus Es for repeated loading was nearly in proportion to deviator stress (fig. 4). Deformability D for static virgin loading was 0.05 to 0.15 times of Es (fig. 5). Besides, the ratio of Ed to Es at the frequency of 1 to 6 hz was about 1.2 to 8.0 and decreased with static deviator stress (fig. 6). The values of E and η were calculated as dynamic viscous properties by the Voigt model (fig. 2). The test results were applied to three

* Central Research Institute of Electoric Power Industry, Abiko City, Chiba Pref., Japan

dimensional dynamic response analysis.

2. Viscosity in a finite element

Coefficient of viscosity η is introduced in each finite element as follows. The dynamic viscous properties can be represented by the Voigt model.

$$\sigma = E\cdot\varepsilon + \eta\frac{d\varepsilon}{dt} = E\cdot\varepsilon + \lambda\frac{E(1-\nu)}{(1+\nu)(1-2\nu)}\frac{d\varepsilon}{dt}$$

in which

$$\lambda = \frac{(1+\nu)(1-2\nu)}{E(1-\nu)}\eta$$

By means of the principle of virtual work, the equation of motion is reduced among nodal force f^e, nodal displacement δ^e and nodal displacement velocity $d\delta^e/dt$. Damping matrix of a finite element therefore can equate to $c^e=\lambda k^e$ and λ can be estimated from η.

3. Dynamic modal analysis by means of three dimensional finite element method

Six tetrahedron finite elements were made up to a hexahedron element (fig. 7). It was investigated that Givens-Householder method was most suitable in various methods for solving eigen value equation with 200 or more dimensions. Then natural periods and modes of several low orders were calculated by the method. The damping constant hn of n-th vibration mode is obtained from the equation hn = Cn/2WnMn, in which $Cn = \{\phi\}^T n\,[C]\{\phi\}n$. Wn is natural angular frequency and $\{\phi\}n$ is n-th mode vector.

4. Three dimensional seismic analysis of rock fill dam (table 1)

Numerical analysis was carried out for three dams (fig. 8). A-dam is constructed on the V-shape valley and B-dam is relatively high and C-dam is low but is situated on the U valley with plain bottom and has asphalt-facing steep slope. Distribution of dynamic Young's modulus in dams (fig. 10) was estimated considering the void ratio (fig. 9) after elasto-plastic analysis of banking. And coefficient of viscosity η was estimated according to static deviator stress. Dam body was divided into the assemblage of hexahedron elements having 138 to 170 nodal points within the memory limit of computer.

5. Input acceleration at three dimensional boundary (table 2)

A1 is sinusoidal input acceleration. The amplitude is 100 gal and the frequency is gradually changed from 1 to 10 hz. A2, B1, B2, C1 and C2 are based on observed random accelerations with power spectra (fig. 12). A2, B2 and C2 have characteristics of dominant frequency nearly equal to first natural frequency of the dam. Values of maximum acceleration of inputs at the boundary are equal 100 gal.

6. Vibration mode (fig. 11)

The 1st mode presents shear vibration perpendicular to dam axis and the 2nd mode shows shear vibration parallel to dam axis. Modes are different with the shape of the valley. At A-dam and B-dam situated on the V-shape valley, the 3rd mode presents vertical vibration. On the other hand, at C-dam on the U-shape the 3rd mode is higher order of vibration perpendicular to dam axis.

7. Natural period (table 2)

High B dam has 1st natural period of 0.64 sec which is the longest of three dams. Secondary, U-shape and steeper C dam has 0.56 sec in spite of low dam. Then A dam with middle height has the shortest 1st natural period. From this, the natural period of a dam is not only affected by height but also by shape of the valley.

8. Damping (table 2 and table 3)

Damping depends not only on η but on E. The value of h_1 for the 1st mode is calculated 8 to 13 per-cent. The order of made is the higher, the damping value is larger.

9. Acceleration response

Amplitudes of acceleration response against input accelerations perpendicular to dam axis and parallel to dam axis are respectively shown in fig. 13 and fig. 14. Amplification for sinusoidal input A1 grows especially and is about 2 times of amplifications for random input A2 (fig. 14). In B2 and C2 random inputs with the excellent period nearly equal to this of the dam, the values of the acceleration at the top of dams are amplified to about 390 gal.

10. Dynamic deformation (table 2)

Deformations against input acceleration perpendicular to dam axis were calculated 0.7 to 3.3cm and those against one parallel to dam axis were about 80 per-cent of the above value.

11. Conclusion

Dynamic tensile stress is apt to occur near the slope surface and it is concluded that upper one-third slope should be carefully compacted or porously pre-pacted by poor cement-mortar in order to give some cohesion of about 0.5 to 1.0 kg/cm^2. Comparing between dynamic horizontal stresses in two dimensional analysis and those in three dimensional analysis, three dimensional stresses are calculated smaller. It is because the restraint of deformation at the perimeter of dam can be taken into account in three dimensional analysis. Distribution of acceleration response during earthquake parallel to dam axis is presented in fig. 17 and dynamic horizontal tensile stress occures as shown in fig. 18. Dynamic tensile stress, which is careful of seepage flow through the dam, is concentrated near the top of dam. And dynamic earth pressure in direction of dam axis acts to the wall of spillway situated at the side of the dam. It is concluded that such the tensile dynamic stress should be resisted by well compacted soil core or injected cohesive material near the abutment of dam.

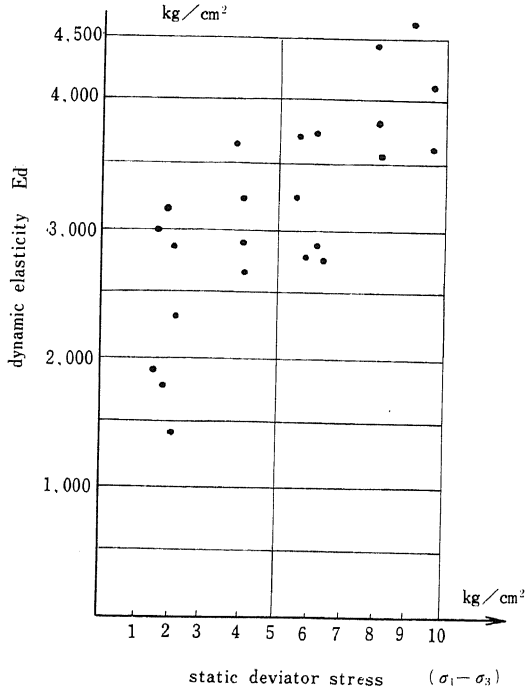

Fig. 1 Dynamic Modulus of Deformability for Repeated Loading Ed against Static Deviator Stress

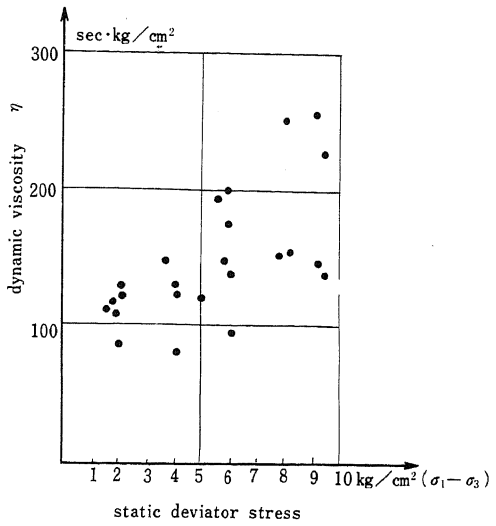

Fig. 3 Dynamic Coefficient of Viscosity η against Static Deviator Stress

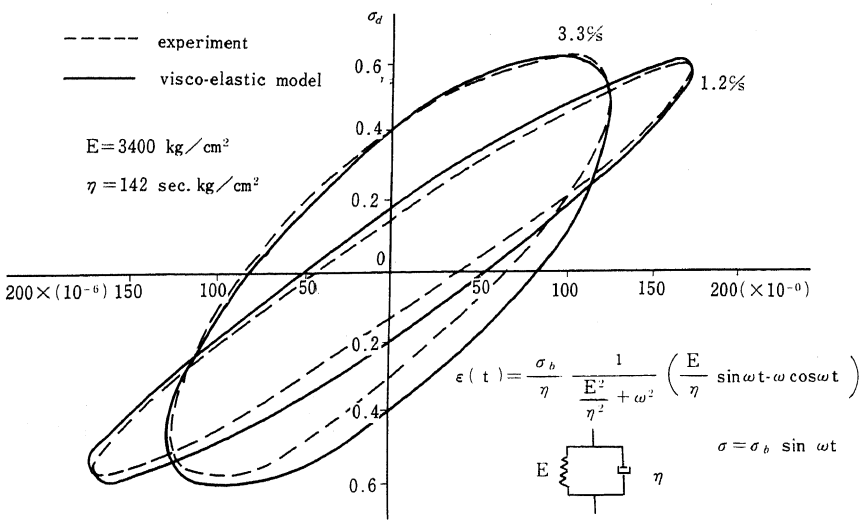

Fig. 2 Dynamic Hysterisis Loop of Rock Fill Material

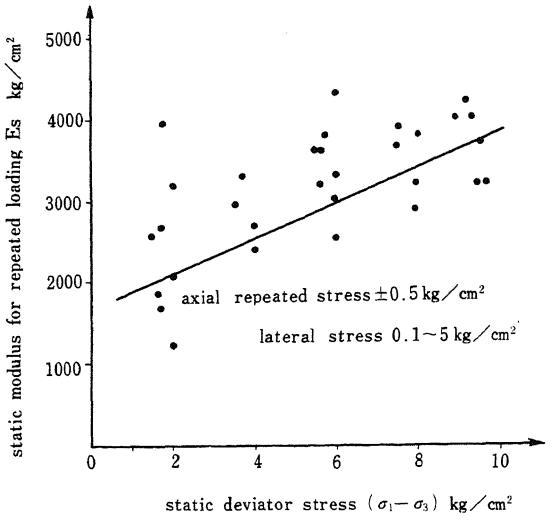

Fig. 4 Static Modulus for Repeated Loading against Deviator Stress

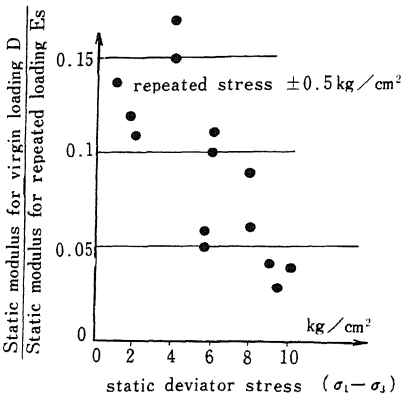

Fig. 5 Ratio of Static Moduli of Deformability for Virgin loading D to Repeated loading Es depending on Static Deviator Stress ($\sigma_1-\sigma_3$)

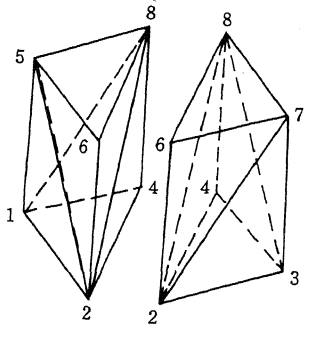

tetrahedron	node		
①	5	8	1
②	5	8	2
③	1	8	4
④	6	8	2
⑤	2	8	3
⑥	2	8	4

Fig. 7 Hexahedron composed from six Tetrahedrons

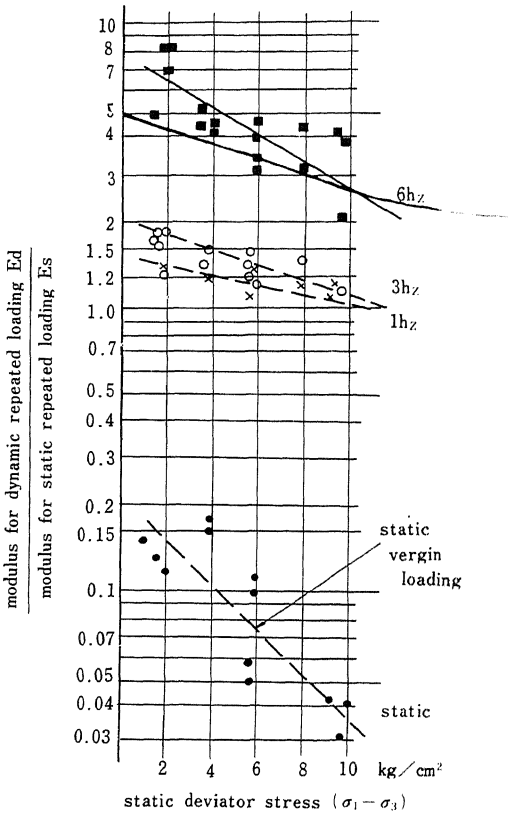

Fig. 6 Ratio of Dynamic Moduli Ed to Static Modulus for Repeated Loading Es depending on Frequency and Static Deviator Stress

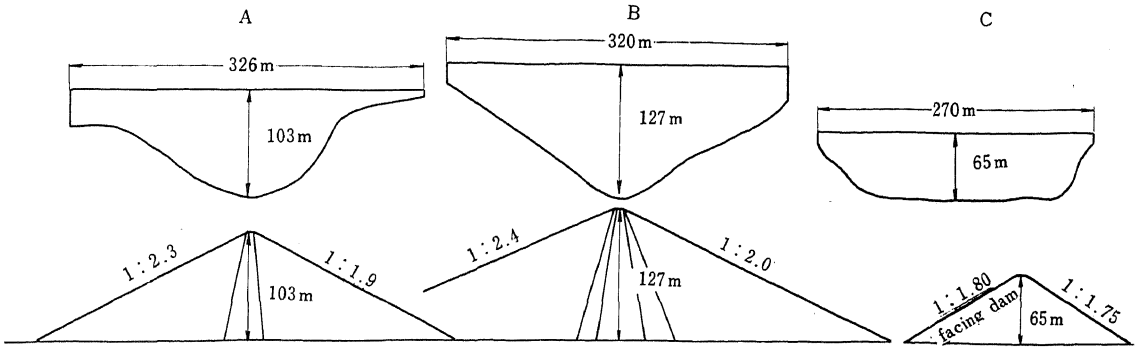

Fig. 8 Three Dams analyzed by Three Dimensional Modal Analysis

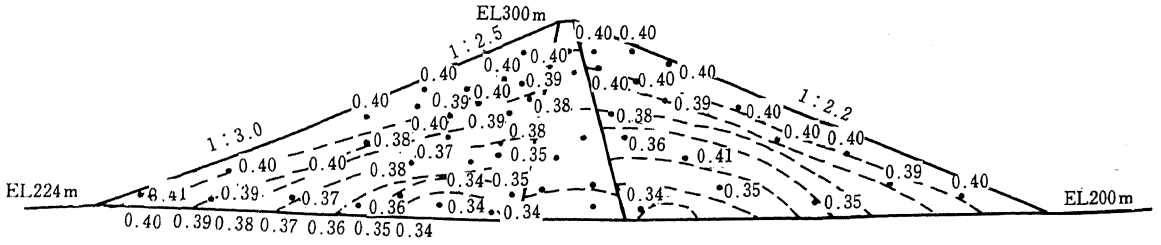

Fig. 9 Calculated Void Ratio after Banking by means of the Successive Elasto-Plastic Analysis

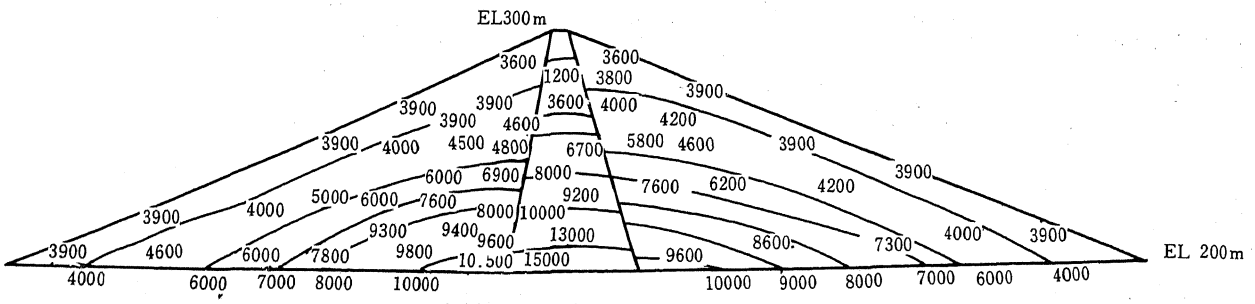

Fig. 10 Dynamic Young's Modulus estimated by Void Ratio and Dynamic Material Test (kg/cm^2)

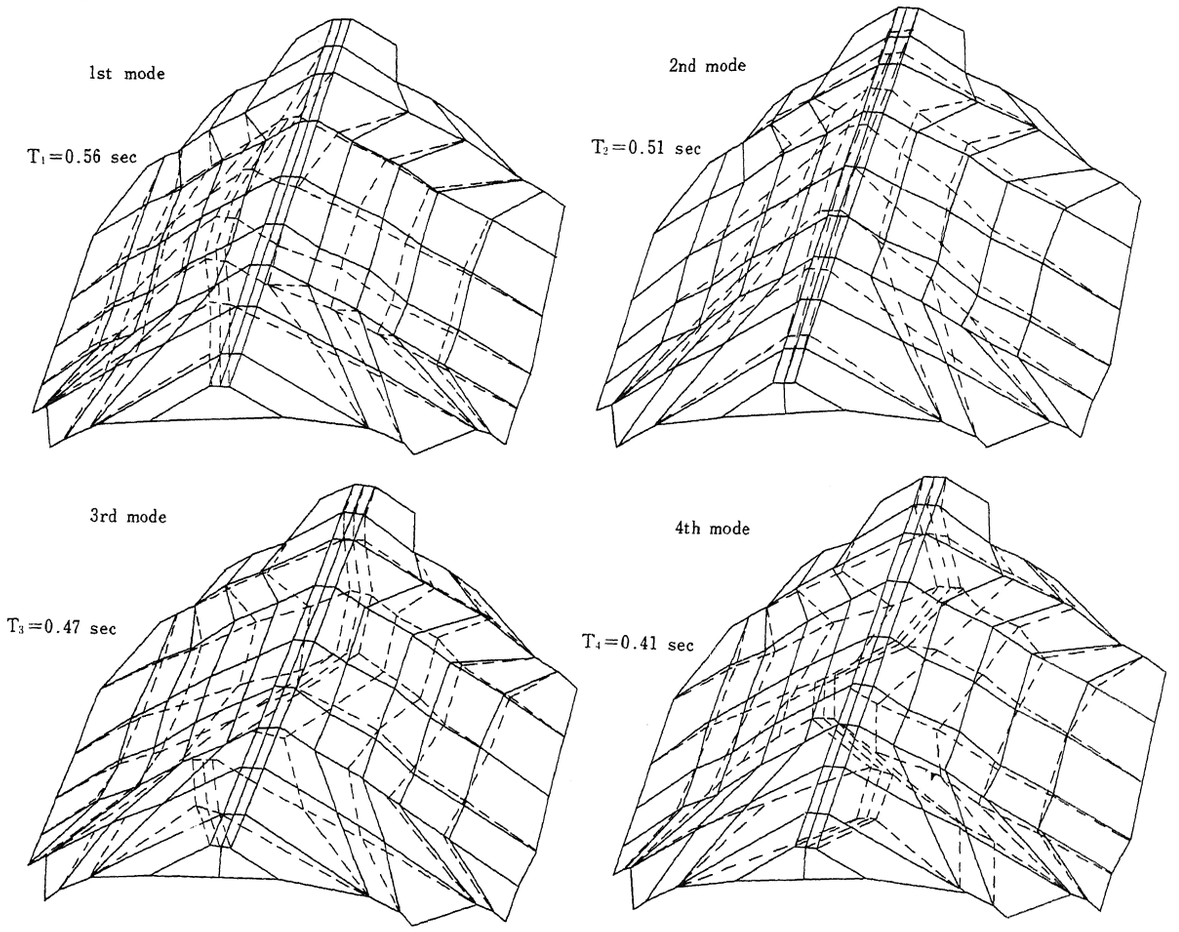

Fig. 11 Vibration Modes (1st: perpendicular to dam axis, 2nd: parallel to dam axis, 3rd and 4th: higher modes of 1st mode) : C dam

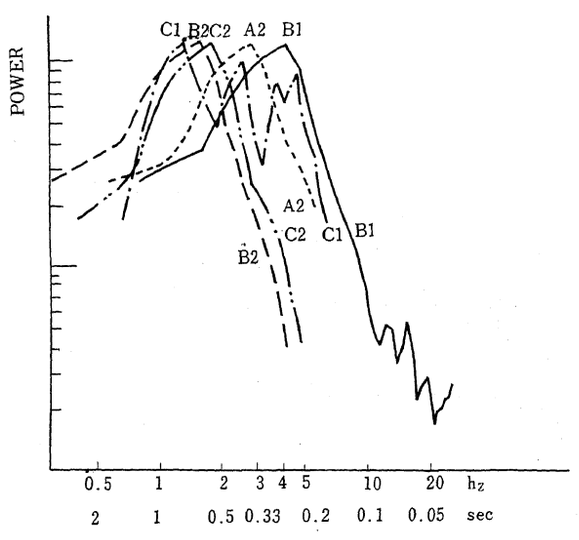

Fig. 12 Power Spectra of Input Accelerations

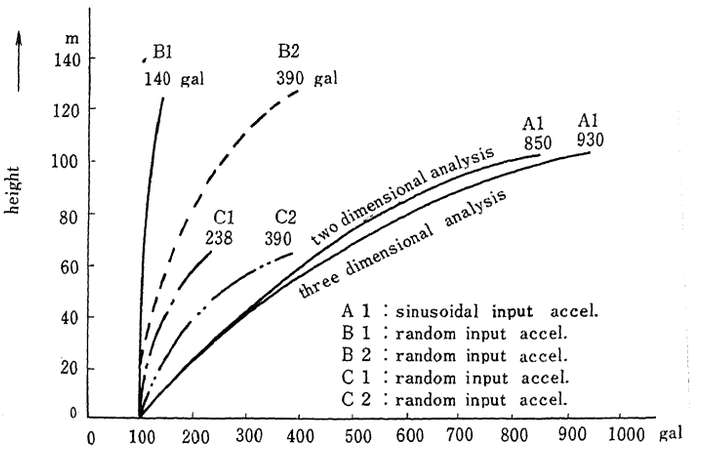

Fig. 13 Amplitudes of Accelerations in Several Kinds of Input Accelerations perpendicular to Dam Axis

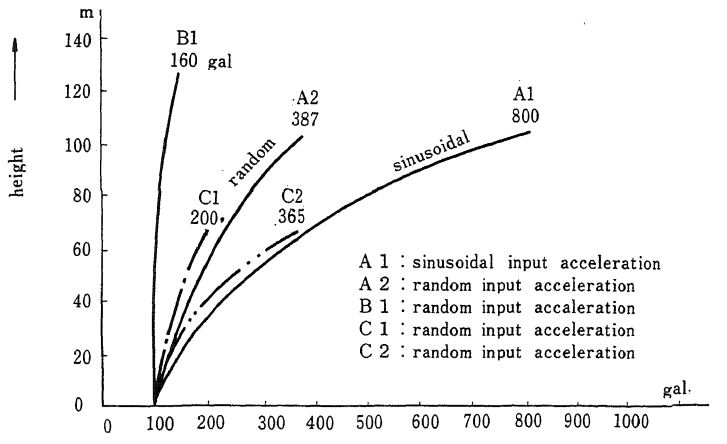

Fig. 14 Amplitudes of Accelerations in Several Kinds of Input Accelerations parallel to Dam Axis

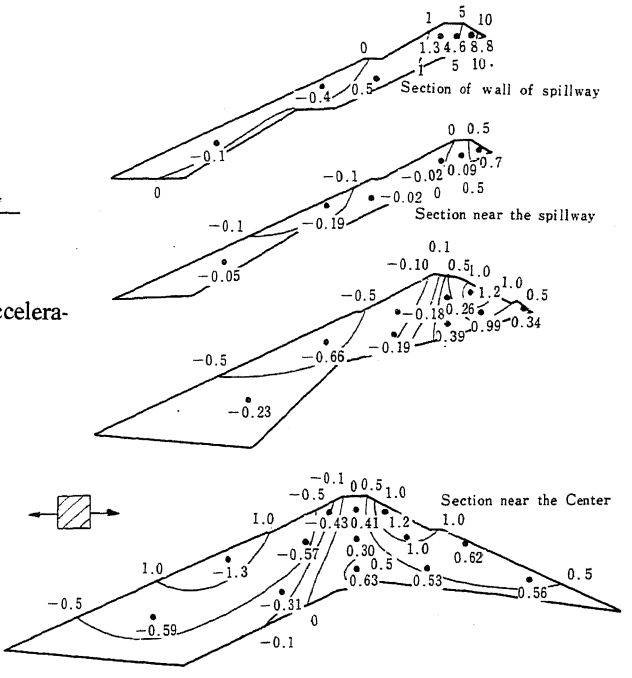

Fig. 15 Dynamic Stress (kg/cm^2) in Several Vertical Sections in Earthquake A1 perpendicular to Dam Axis

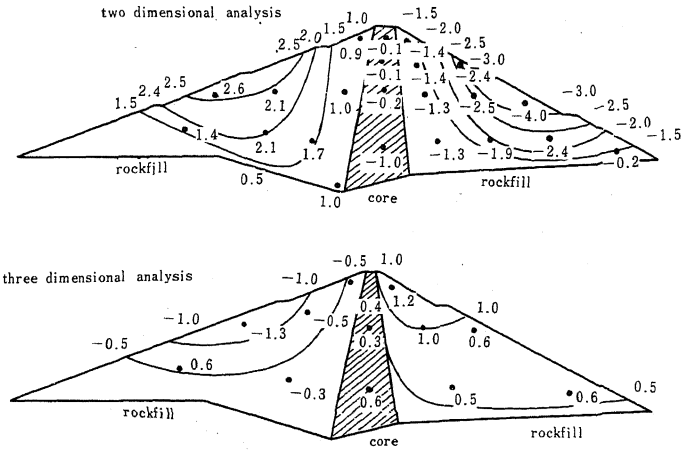

Fig. 16 Comparison of Dynamic Horizontal Stresses (kg/cm^2) in two and three Dimensional Analyses in Earthquake A1 perpendicular to Dam Axis

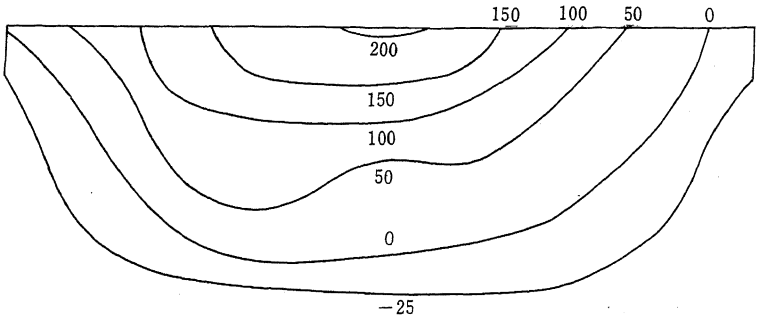

Fig. 17 Horizontal Acceleration (gal) in Up Stream Face during Earthquake C1 parallel to Dam Axis

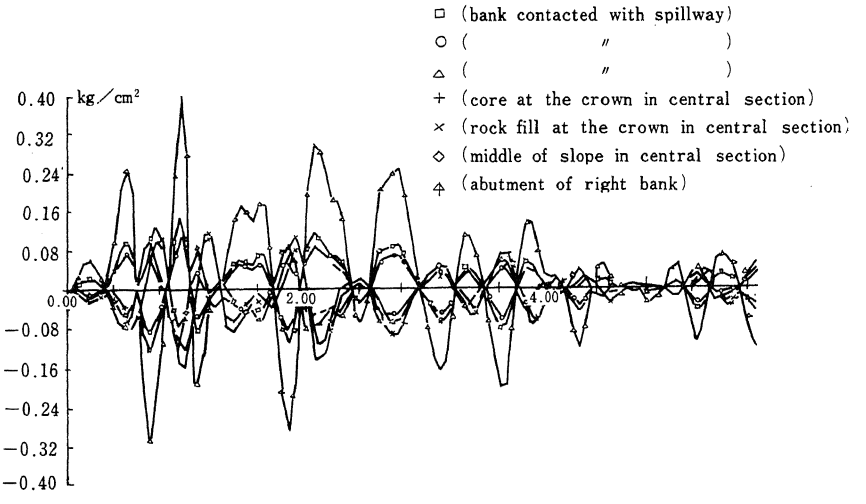

Fig. 19 Time History of Dynamic Horizontal Stresses (kg/cm^2) near the Side Spillway in Earthquake A2 parallel to Dam Axis

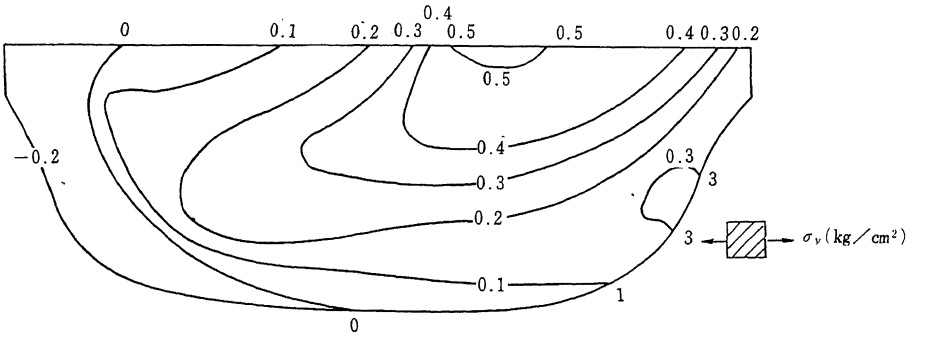

Fig. 18 Dynamic Horizontal Stresses (kg/cm^2) in Upstream Face during Earthquake C1 parallel to Dam Axis

table 1

	analyzed dams		
	A-dam	B-dam	C-dam
height	103 m	127 m	65 m
span	326 m	320 m	270 m
slope of up stream face	1 : 2.3	1 : 2.4	1 : 1.8
slope of down stream face	1 : 1.9	1 : 2.0	1 : 1.75
dynamic young's modulus	5000 ~ 15000 Kg/cm^2	3000 ~ 10000 Kg/cm^2	3800 ~ 6500 Kg/cm^2
dynamic viscous coefficient	150 Sec. Kg/cm^2	110 ~ 210 Sec. Kg/cm^2	162 ~ 195 Sec. Kg/cm^2
nodal points	152	138	170

table 2

Dam							
shape (fig. 8)			A		B		C
natural period	1st	(sec)	0.39		0.64		0.56
	2nd	(sec)	0.35		0.57		0.51
	3rd	(sec)	0.32		0.51		0.47
damping constant	1st		0.08		0.12		0.13
	2nd		0.10		0.13		0.15
	3rd		0.10		0.15		0.17
Input earthquake							
spectrum (fig. 12)			A1	A2	B1	B2	C_1	C_2
dominant period		(sec)	varing sinnsoidal	0.34	0.25	0.64	0.2	0.55
max. acceleration		(gal)	100	100	100	100	100	100
Response against earthquake perpendicular to dam axis								
max. horizontal accel.		(gal)	930		140	390	238	390
max. vertical accel.		(gal)			20	35	25	43
max. horizontal disp.		(cm)	1.4		0.7	3.3	1.7	3.0
max. vertical disp.		(cm)					0.1	0.3
max. dynamic tensile stress (Kg/cm^2)			1.4		0.1	0.3	0.2	0.2
Response against earthquake parallel to dam axis								
max. horizontal accel.		(gal)	800	387	160		200	365
max. vertical accel.		(gal)	180	90	35			
max. horizontal disp.		(cm)	2.4	1.1	0.6		1.3	2.3
max. vertical disp.		(cm)	0.5	0.1	0.1			
max. dynamic tensile stress (Kg/cm^2)			0.6	0.5	0.4		0.5	0.8

Table 3

order	natural period Tn	damping coefficient hn	order	natural period Tn	damping coefficient hn
1	0.641	0.116	9	0.372	0.210
2	0.565	0.130	10	0.367	0.206
3	0.508	0.145	11	0.352	0.219
4	0.430	0.175	12	0.351	0.203
5	0.417	0.178	13	0.345	0.232
6	0.413	0.183	14	0.332	0.238
7	0.394	0.204	15	0.320	0.244
8	0.388	0.191			